arXiv:1702.02683v1 [nlin.PS] 9 Feb 2017

Localized Faraday patterns with inhomogeneous parametric excitation

Héctor Urra,[1,2,*] Saliya Coulibaly,[3,†] Leonardo Gordillo,[2,4,‡] and Mónica A. García-Ñustes[1,§]

[1] *Instituto de Física, Pontificia Universidad Católica de Valparaíso, Casilla 4059, Chile*
[2] *Departamento de Física, Facultad de Ciencias Físicas y Matemáticas, Universidad de Chile, Casilla 487-3, Santiago, Chile*
[3] *Université de Lille, CNRS, UMR 8523 - PhLAM - Physique des Lasers Atomes et Molécules, F-59000 Lille, France.*
[4] *Department of Chemical Engineering and Materials Science, University of Minnesota, Minneapolis, Minnesota 55455, USA*

Faraday waves are a classic example of a system in which an extended pattern emerges under spatially uniform external forcing. Motivated by systems in which uniform excitation is not plausible, we study both experimentally and theoretically the effect of inhomogeneous forcing on Faraday waves. Our experiments show that vibrations restricted to finite regions lead to the formation of localized subharmonic wave patterns, whose localization depends on the extent of the excited region. The prototype model used for the theoretical calculations is the parametrically driven and damped nonlinear Schrödinger equation, which is known to describe well Faraday-instability regimes. For an energy injection with a Gaussian spatial profile, we show that the evolution of the envelope of the wave pattern can be reduced to a Weber-equation eigenvalue problem. Our theoretical results provide very good predictions of our experimental observations provided that the decay length scale of the Gaussian profile is much larger than the pattern wavelength.

PACS numbers: 05.45.Yv, 05.45.-a, 89.75.Kd

Patterns formation is a major area of nonlinear dynamics [1, 2]. During the last decades, a major progress has been achieved in understanding how an extended system with homogenous conditions can spontaneously undergo from a basic homogeneous state to a self-organized one [3, 4]. However, the homogeneity of parameters is often an ideal concept. Indeed, many physical systems are inherently subject to small variations of their features or can be designed with built-in heterogeneities. In this case, the implications in the dynamical behavior of the system can be relevant. In particular, if the pumping energy (forcing) is not uniform, the system can develop localized structures. A dramatic example of this behavior is a tsunami, a series of waves formed by the displacement of a large volume of water, usually caused by an earth sudden movement [5]. The injection of energy is localized despite spatially spread tsunami consequences. In a smaller scale, swimmers can inject energy into their surroundings as they advance through the water, causing surface disturbances that may have an important effect on their drag [6, 7]. In both cases, the localized injection of energy possesses an important role on further dynamics. From the point of view of patterns formation, the impact of heterogeneity in the energy injection includes modification of instabilities domains, threshold discretization [8–11] just to cite a few. In particular, the concept of global mode have been introduced to characterize the synchronized response of such a system to the locality of the driving.

In out-of-equilibrium systems such as parametrically forced ones, the injection of energy plays a fundamental role in formation of patterns. Parametric forcing consists on driving a system close to twice its natural frequency. Initially observed in vertically vibrated Newtonian fluids [12, 13], Faraday-wave-like structures can be encountered in nonlinear lattices [14], optical fibers [15], Kerr-type optical parametric oscillators[16], easy-plane ferromagnetic materials exposed to oscillatory magnetic fields [17, 18] and parametrically driven damped chains of pendula [19].

Inhomogeneities in parametrically forced systems have been considered in different contexts. Local defects [19, 20], finite-size effects[21, 22], linear-depth gradients in a water trough [23, 24] and Gaussian parametric injection in optical systems[25] are some examples. Likewise, proper tuning of inhomogeneous parameters allow to engineer the outcome of an out-of-equilibrium systems with evident technological applications [26, 27].

In this letter, we study both experimentally and theoretically the Faraday instability generated by localized forcing. Our experimental setup consists of a water channel with deformable bottom. The system is theoretically modeled by the parametrically driven nonlinear Schrodinger equation (PDNLS) [12, 13] with spatial varying forcing parameter. Assuming a Gaussian profile for the injection, we use a WKBJ scaling technique [9] to derive an eigenvalue Weber equation that governs the envelope of the patterns. Consequently the response of the system is discrete and the system solutions are shown to be Hermite polynomials with Gaussian modulation.

Experimental setup and measurement protocol: Our experimental setup is composed of a transparent rectangular water channel of 15-mm long, 490-mm wide and 100-mm deep, whose bottom has a central soft region 240-mm wide manufactured in a soft silicone-elastomer (Shore hardness OO). The assembly rests over a system of 13 pistons evenly spaced ($\Delta x = 16\,\mathrm{mm}$, each of them restricted to vertical motion by two fixed axial bearings. At the bottom of each piston, we assembled a tiny roller to

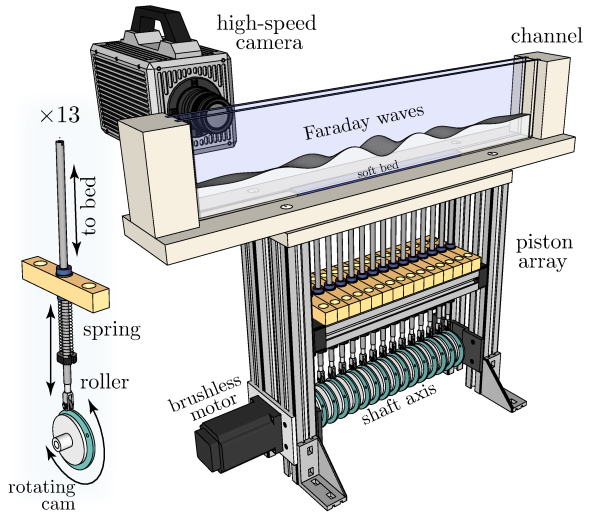

Figure 1. (Color online) Experimental setup used to generate a localized injection of energy in a Faraday-wave configuration. The soft bottom is attached to a set of pistons, each linked to a rotary cam system attached to a common shaft and a brushless motor. Amplitude and frequency can be independently programmed.

be used as a follower. Using compressed springs, the pistons are pushed towards a set of rotary cams placed in a common horizontal axis. The axis is respectively coupled to a brushless motor with feedback (Model BLM-N23-50-1000-B). The system resembles a music-box transmission

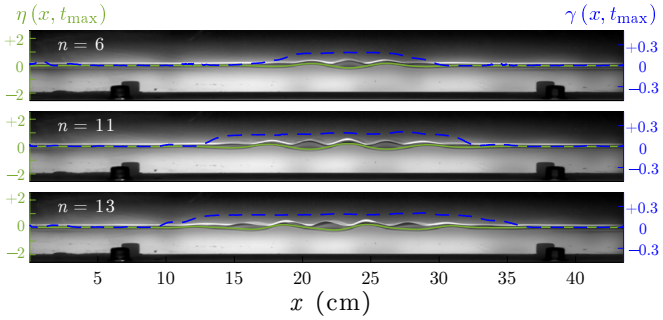

Figure 2. (Color online) Snapshots of the observed structures under localized forcing for different excitation regions: From top to bottom $\sigma_i = 96, 176, 208$ mm. Green continuous lines depict the detected free-surface deformations at the wall, while blue dashed curves, the profiles of the effective acceleration at the surface.

system as shown in Fig. 1 and allows to deform the bottom of the channel with a spatial distribution. Cams are shaped in such a way that an oscillatory angular motion creates a vertical oscillatory motion in the piston. In this way, both the amplitude and frequency of oscillations can be easily programmed through the motor controller. The motion of any piston can be easily switched off by changing our special cams to circular ones.

The channel trough was filled with a Photoflo-water solution (concentration: 2%) up to 20-mm deep. Under uniform forcing (e.g. frequency $f = 14.86$ Hz), Faraday waves emerge above an acceleration threshold of $\Gamma_c = 0.3$. The waves display a central node in the cross-wise direction. The emerging waves were visualized using a high-speed camera. The channel was front illuminated in such a way that a clear vertical cut of the flow at the wall can be observed. A small amount of white dye was added to the solution to improve visualization.

Our measurement protocol was the following: First, we chose the frequency in such a way that the wavelength of the Faraday waves matches the inter-piston distance. Starting from the maximum number of excited pistons, i.e. $n = 13$, we acquired a sequence of highly resolved images in both space and time. Then, we sequentially decreased the number of excited pistons, hence reducing the excitation region. In Fig. 2, we display typical images of the observed waves for different numbers of excited pistons. The snapshots include also the reconstructed free-surface deformation at the wall $\eta(x,t)$ and the profile of the effective acceleration at the surface $\Gamma(x,t)$, at $t = t_{\max}$, *i.e.* when maximal deformations are observed through the whole cycles [28]. Both curves were obtained using standard edge-detection algorithms. Examples of the full spatiotemporal evolution of the free-surface are plotted in Fig. 3.

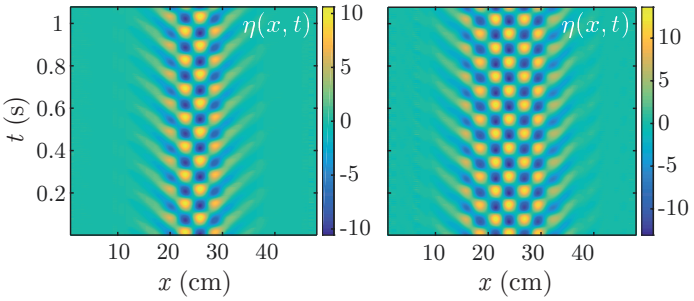

Figure 3. (Color online) Spatiotemporal evolution of free surface (Faraday waves) at the wall $\eta(x,t)$ for $n = 6$ pistons (left) and $n = 13$ pistons (right).

As shown in Figs. 2 and 3, the excitation of a reduced bottom region generates wave patterns that are spatially localized. The patterns oscillate at half the forcing frequency (parametric instability), which is the Faraday-waves signature. The observed patterns, that we will refer to as *localized Faraday waves,* have a standing-wave core that emits spatially decaying waves toward the unperturbed regions. To characterize the wave localization, we perform the following analysis on $\eta(x,t)$: First, we apply the temporal Fourier transform and extract the phase and amplitude for the dominant frequency $f/2$. In the standing-wave region, the wave displays a constant phase along x that decreases linearly as we enter into the wave-emission region. The amplitude on the other hand, displays a smooth decay in the wave-emission re-

gion but a serrated shape on the standing-wave. The spatial envelope of the amplitude for the whole domain was obtained by fitting a Gaussian curve on the amplitude local maxima of the standing-wave region and the remaining tails of the wave-emission one. The width of the envelope is defined as $\sigma_w \equiv$ HWHM, i.e. the half width at half maximum. Likewise, to characterize the injection localization, we obtained the envelope of $\Gamma(x,t)$ and straightforwardly obtain the HWHM, σ_i. The two quantities, the wave-envelope width σ_w and the injection-envelope width σ_i, were measured for runs with different number of pistons. Results are summarized in Table I and displayed in Fig. 4.

n	Γ	σ_i (mm)	σ_w (mm)	n	Γ	σ_i (mm)	σ_w (mm)
6	0.443	48	42	10	0.382	69	66
7	0.453	54	46	11	0.382	72	74
8	0.392	61	51	12	0.382	73	85
9	0.382	68	57	13	0.382	80	92

Table I. The table shows the set of our experiments including the forcing amplitude Γ, the width of the injection region σ_i and width of the wave envelope σ_w. In all cases, $f = 14.86$ Hz. Errors estimated from the confidence intervals of the fitted parameters are negligible ($\lesssim 0.5$ mm).

Theoretical description of localized Faraday waves: The prototype model describing the dynamics of unidimensionally extended systems in the vicinity of Faraday instability is the parametrically driven and damped nonlinear Schrodinger equation,

$$\partial_{t'} A = -i\nu A - i|A|^2 A - i\partial_{xx} A - \mu A + \gamma \bar{A}. \qquad (1)$$

where $A(x,t)$ stands for the complex envelope of the standing waves and $\bar{A}$ its complex conjugate; x and t are the dimensionless space and time respectively. Besides, ν is the detuning parameter which measures the offset to the parametric resonance, μ the damping parameter, and γ stands for the forcing amplitude of the parametric forcing. The relation between the experiment quantities and the dimensionless parameters ν, μ, γ, as well as the time and length scaling laws, are given in detail in Refs. [12, 29]. Notice that the PDNLS equation (1) applies only in the limit $\nu \sim \mu \sim \gamma \ll 1$. For $\gamma > \mu$, $\nu > 0$ and $\gamma^2 < \nu^2 + \mu^2$, the system exhibits subharmonic patterns with critical wavelength $k_c = \pm\sqrt{\nu}$, i.e., Faraday waves.

We extend Eq. (1) to inhomogeneous systems by assuming that $\gamma \equiv \gamma(x)$ is a function describing the spatial profile of the forcing. We linearize Eq. (1) around the trivial homogeneous steady state and analyze the obtained equation and its complex conjugate (for details, see Supplemental Material [30]). When $\gamma(x)$ is a slowly varying function of the space, we obtain after some algebra:

$$\left[(\partial_t + \mu)^2 + (\nu + \partial_{xx})^2\right] A - \gamma(x) A = 0. \qquad (2)$$

Following our experimental results, see e.g blue dashed lines in Fig.2, we assume that the injection profile γ is a localized function satisfying three key features: i) $\gamma(x)$ is symmetric with respect to some x_0, ii) $\gamma(x)$ has a single extremum at x_0 with non-vanishing second derivative, iii) decays to 0 as $x \to \pm\infty$. For the sake of simplicity, we choose $\gamma(x)$ to be a Gaussian function:

$$\gamma(x) = \gamma_i \exp\left(-\frac{x^2}{2\sigma_i^2}\right), \qquad (3)$$

where γ_i is the forcing amplitude and σ_i is a dimensionless standard deviation. The degree of inhomogeneity of the system can be modeled through the parameter $\varepsilon \equiv 1/\sigma_i$, which should be small to satisfy the condition of slow spatial dependence in $\gamma(x)$. In the original physical variables, it can be shown that $\varepsilon \ll 1$ is equivalent to require that the pattern wavelength λ is much smaller than the variation length-scale of the forcing. Notice that this assumption is in agreement with our experimental observations.

Introducing the slowly varying variable $X \equiv \varepsilon x$, Eq.(3) becomes:

$$\left[(\partial_t + \mu)^2 + \left(\nu + \varepsilon^2 \partial_{XX}\right)^2\right] A - \gamma^2(X) A = 0, \qquad (4)$$

where $\gamma(X) = \gamma_i\left(1 - \frac{1}{2}X^2\right)$ is the series expansion of γ. This equation can be solved using the procedures detailed in refs. [8–11, 31]. As shown in the Supplemental Material at [30], the solution of (4) can be expressed in terms of a carrier wave (wavelength $\sqrt{\nu}$ at dominant order) and an envelope A_0 ($y \equiv \sqrt{\varepsilon}x$), which obeys:

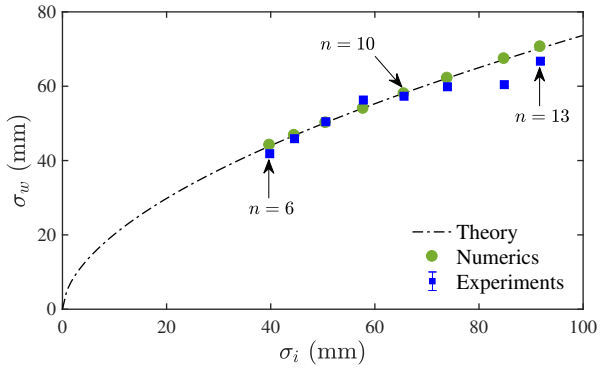

Figure 4. Color Online: Injected forcing variance σ_i as a function of pattern variance σ_p for $\nu = 0.07$ and $\mu = 0.0152$. Theoretical (solid black line), experimental (blue squares) and numerical (green circles) data are depicted.

$$\partial_y^2 A_0 + \left(\beta^2 - \alpha y^2\right) A_0 = 0, \qquad (5)$$

where $\alpha \equiv \mu^2/4\nu$ and $\beta^2 \equiv \mu(\gamma_1/2\nu + i\omega_1/2\nu)$. Here γ_1 and ω_1 have been introduced as:$\gamma \simeq \mu + \varepsilon\gamma^{(1)}$, $\omega \simeq \varepsilon\omega^{(1)}$. Equation (5) is a linear eigenvalue problem with a

discrete set of solutions $A_{0,m}(y)$, each given in terms of the m-th Hermite polynomial H_m modulated by a Gaussian function; i.e. $A_{0,m}(y) = H_m\left(\alpha^{1/4}y\right)e^{-\left(\sqrt{\alpha}/2\right)y^2}$. The eigenvalue problem also requires $\beta^2/\sqrt{\alpha} = 2m+1$. It is straightforward to see that the related quantities $\gamma_m^{(1)} = (2m+1)\sqrt{\nu}$ and $\omega_m^{(1)} = 0$ are now discrete. Likewise, $\gamma_m = \mu + (2m+1)\left(\frac{\sqrt{\nu}}{\sigma_i}\right), \omega_m = 0$. We can infer that the first emerging mode in our experiments is the fundamental one ($m = 0$), which in terms of x reads:

$$A_0(x) = e^{-\frac{x^2}{2\sigma_w^2}}, \quad \text{with } \sigma_w = \left(\frac{\sqrt{\nu}}{\mu}\sigma_i\right)^{1/2}. \qquad (6)$$

Notice that all the solutions derived from (4), including the fundamental mode (6), display localization, which is the key qualitative feature of localized Faraday waves. The theory also predicts an increase of the instability threshold γ_m^c for every mode including the fundamental one, *i.e.* $\gamma_m^c = \mu + \sqrt{\nu}(2m+1)/\sigma_i$. Furthermore, equation (6) shows that the width of the envelope A_0 scales as the square root of the injection-region width, which is a feature that can be tested on the experimental data in Fig. (4).

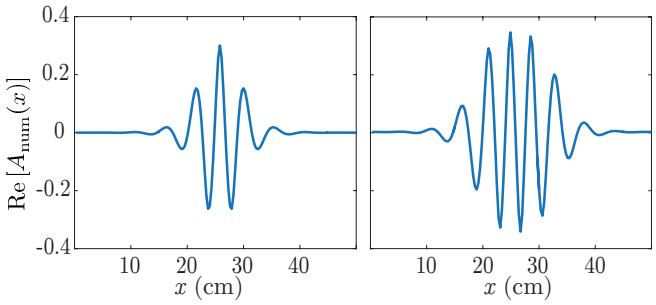

Figure 5. (Color online) Numerical profile of the real part of a typical Faraday pattern profile Re$(A(x,t))$ for $n = 6$ pistons (left) and $n = 13$ pistons (right) obtained using Eq. (1) with $(\mu, \nu, \gamma) = (0.0156, 0.070, 0.0694)$.

To make quantitative comparisons, we need first to determine the dimensionless quantities of Eq. (1) in terms of experimental parameters. The formulas provided in [12, 29] can be used to directly compute γ_i and ν. The formulas available in the literature for the damping coefficient μ however seem to be not appropriate for our experimental conditions. Hence we considered μ as an adjustable parameter, which we estimated by fitting (6) on the experimental data of Fig. 4. To test the validity of our results we fitted a power law $\sigma_w = a\sigma_i^p$ and found $(a, p) = (2.27, 0.480)$. The exponent p is remarkably consistent with the predicted square-root dependence in 6.

As a final check, we also performed direct numerical simulations of Eq. (1) with $\gamma(x)$ given by the expression (3). The goal was to determine if the linear approximation we did to obtain Eq. 4 remained valid for the set of $(\mu, \nu, \gamma, \sigma_i)$ that we chose. Using a Gaussian function centered in a 170-point spatial grid with resolution d$x = 0.3$, we ran a simple Runge-Kutta scheme on (1). To illustrate the results, we plot in Fig. 5 two numerical solutions for the Faraday wave profile Re$(A(x,t))$ under localized injection with two different σ_i values (correspoding to 6 and 13 pistons). The results are very consistent: the theory does not only match well the full-numerical simulation but also the experimental results as shown in Fig. 4.

In conclusion, we designed an experimental setup with a controlled spatial energy injection consisting of a quasi one-dimensional rectangular water channel with a soft deformable bottom. Localized patterns were observed in the Faraday instability region, suggesting that the profile of the effective injection displays a localized function with decaying tails. Assuming that the width of the injection region is larger than the characteristic pattern wavelength we developed a WKBJ approximation on the prototype model describing our experiment. We have successfully derived the spatial law of the observed patterns. The results presented here might be helpful to understand the impact of parameter inhomogeneities on pattern-formation processes in all extended physical systems. Studies to characterize spatiotemporal dynamics of patterns are in process.

M.A.G-N. thanks for the financial support of FONDECYT projects 11130450. L. G. was partially supported by Conicyt/Becas Chile de Postdoctorado 74150032. M.A.G-N. and S.C. thank ECOS-Sud n° C15E06.

* hector.ignacio.rurra@gmail.com
† saliya.coulibaly@univ-lille1.fr
‡ lgordill@ing.uchile.cl
§ monica.garcia@pucv.cl

[1] G. Nicolis, I. Prigogine, *et al.*, *Self-organization in nonequilibrium systems*, Vol. 191977 (Wiley, New York, 1977).
[2] M. C. Cross and P. C. Hohenberg, Rev. Mod. Phys. **65**, 851 (1993).
[3] M. Cross and H. Greenside, *Pattern formation and dynamics in nonequilibrium systems* (Cambridge University Press, 2009).
[4] L. M. Pismen, *Patterns and interfaces in dissipative dynamics* (Springer Science & Business Media, 2006).
[5] J. L. Hammack, J. Fluids Mech. **60**, 769 (1973).
[6] E. Raphaël and P. G. de Gennes, Phys. Rev. E **53**, 3448 (1996).
[7] A. Benusiglio, F. Chevy, É. Raphaël, and C. Clanet, Phys. Fluids **27**, 072101 (2015).
[8] S. Coulibaly, *Solliton Dissipatifs des oscillateurs Parámetriques optiques: Instabilités convectives/absolues et effets non-linéaires de walk-off*, Ph.D. thesis, Universite de Lille I (2006).
[9] P. Huerre, Annu. Rev. Fluid Mech. **22**, 473 (1990).

[10] M. N. Ouarzazi, P. A. Bois, and M. Taki, Phys. Rev. A **53**, 4408 (1996).
[11] P. A. Monkewits, P. Huerre, and J.-M. Chomaz, J. Fluid Mech. **251**, 1 (1993).
[12] J. W. Miles, J. Fluid Mech. **148**, 451 (1984).
[13] J. Miles and D. Henderson, Annu. Rev. Fluid Mech. **22**, 143 (1990).
[14] B. Denardo, B. Galvin, A. Greenfield, A. Larraza, S. Putterman, and W. Wright, Phys. Rev. Lett. **68**, 1730 (1992).
[15] J. N. Kutz, W. L. Kath, R.-D. Li, and P. Kumar, Opt. Lett. **18**, 802 (1993).
[16] S. Longhi, Phys. Rev. E **53**, 5520 (1996).
[17] I. V. Barashenkov, M. M. Bogdan, and V. I. Korobov, Europhys. Lett. **15**, 113 (1991).
[18] M. G. Clerc, S. Coulibaly, and D. Laroze, Europhys. Lett. **97**, 30006 (2012).
[19] N. Alexeeva, I. V. Barashenkov, and G. P. Tsironis, Phys. Rev. Lett. **84**, 3053 (2000).
[20] L. Lu, W. Chen, Y. Zhu, and H. Lin, Chin. Sci. Bull. **49**, 1338 (2004).
[21] M. G. Clerc, S. Coulibaly, M. A. García-Ñustes, and Y. Zárate, Phys. Rev. Lett. **107**, 254102 (2011).
[22] L. Gordillo and M. A. García-Nustes, Phys. Rev. Lett. **112**, 164101 (2014).
[23] L. Gordillo, T. Sauma, Y. Zárate, I. Espinoza, M. G. Clerc, and N. Mujica, Eur. Phys. J. D **62**, 39 (2011).
[24] Y. Jiaren, Z. Chuanhui, and Y. Jianqiang, Phys. Fluids **4**, 690 (1992).
[25] F. Ye, C. Huang, Y. V. Kartashov, and B. A. Malomed, Opt. Lett. **38**, 480 (2013).
[26] Y. Jia, J. Yan, K. Soga, and A. A. Seshia, J. Micromech. Microeng. **23**, 114007 (2013).
[27] M. A. Foster, A. C. Turner, J. E. Sharping, B. S. Schmidt, M. Lipson, and A. L. Gaeta, Nature **441**, 960 (2006).
[28] The effective acceleration at the surface, which oscillates at f and not at $f/2$, was obtained by imaging the surface of the liquid below the instability threshold. The profile was then rescaled by the amplitude used in the experiments.
[29] L. Gordillo and N. Mujica, J. Fluids Mech. **754**, 590 (2014).
[30] Supplemental material at URL.
[31] G. Dewel and P. Borckmans, Phys. Lett. A **138**, 189 (1989).